


# Military suitability of COTS UAV due to the level of radiated emissions

Rafał PRZESMYCKI<sup>1</sup> \* and Jarosław MICHALAK<sup>1</sup> 

Military University of Technology, ul. Gen. Sylwestra Kaliskiego 2, 00-908 Warsaw, Poland

**Abstract.** The article presents the assessment of the levels of radiated electromagnetic interference by commercial UAVs in the context of their popular use for various military tasks. The test was conducted in the frequency range from 30 MHz to 6 GHz, in an electromagnetically anechoic chamber, in accordance with the procedures provided for this type of checks. Apart from the control frequencies (which of course exceed the standards), it can be said that most of the tested UAVs using brushless motors do not exceed the emission levels specified by the military standard MIL-STD-461G. This opens the way to the use of COTS UAV as a carrier of electronic systems for the tasks of recognizing sources of radio signals in the investigated band.

**Keywords:** commercial UAV; EMI; electromagnetic chamber; military application; MIL-STD-461G.

## 1. INTRODUCTION

In recent years, there has been a dynamic development of applications for unmanned ground and air platforms (unmanned ground vehicle (UGV), unmanned aerial vehicle (UAV)) that fulfill increased functions of their supported prototypes and offer several new possibilities. These platforms can be supervised from the ground by radio or conduct tasks autonomously in accordance with a previously declared mission or by making independent decisions within a certain scope and creating task networks (e.g. flying ad-hoc network (FANET)). Their importance and number are constantly growing (several million UAVs have already been registered in the USA alone). The first attempts to use UAVs date back to the 1920s. Remembering the first combat use of UAVs in the form of the V1 missile used to bomb London during World War II, the current technical solutions of these platforms allow for the following general classification:

- amateur and professional applications,
- weight from several dozen grams to several tons,
- flight altitude from a few meters to several kilometers (above ground level (AGL)),
- flight time from a few minutes to tens of hours,
- range from a few meters to several hundred kilometers,
- monoplanes, multi-rotor, and hybrid solutions,
- single platforms and UAV swarms,
- managed and autonomous platforms.

A rapidly growing range of UAV applications can be observed in both the civilian and military markets. In the context of the intentions of this study and the assessment of the usefulness of COTS UAVs due to radiated interference, military applica-

tions related to reconnaissance and electronic warfare, as well as combat applications, become particularly important.

Their importance in modern armed conflicts is increasing due to the UAV opportunities offered, which can be perceived as crucial for the implementation of the mission. For example, intelligence gathering, surveillance, and reconnaissance (ISR) in real time. Small UAVs can fly at low altitudes and maneuver in ways that larger objects cannot.

For obvious reasons, there are not many publications on this subject, and the popularity of technical solutions can be concluded mainly based on reports at the stage of simulations and laboratory experiments [1–4]. War is also an invaluable source of information, during which small, commercial UAVs are popularly and effectively used for both combat and reconnaissance and rescue purposes [5].

Let us pay attention to radio techniques, which play one of the key roles during operations. In this area, communication applications (e.g. retransmission points) and reconnaissance (e.g. location of enemy emission sources, making radio maps of the area) or rescue (e.g. searching for lost nodes) or rescue applications (e.g. searching for lost nodes) can be mentioned in this area [6–8].

In each of the radio applications, the vital information is the level of the useful signal to the sum of external interference. It is a value that allows the assessment of the degree of service performance in communications, and in reconnaissance devices, it is one of the factors determining their sensitivity and system efficiency.

At this point, it is worth saying a few words about radio interference (EMI) related to the engines used by UAVs. Long-range heavy UAVs do not use battery-powered motors due to their high-power requirements. Most often, these are spark engines that generate a relatively high level of EMI interference. These interferences have been a significant problem for many

\*e-mail: rafal.przesmycki@wat.edu.pl

Manuscript submitted 2023-08-15, revised 2023-11-03, initially accepted for publication 2023-11-27, published in March 2024.

years in technical solutions related to the operation of sensitive radio receivers mounted on board objects with such engines (e.g. [9–12]). Due to the nature of their generation (commutated and induced, mainly spark plug sparks and commutator brushes), these are broadband interferences that negatively affect the entire range of the analyzed frequencies of interest, although a decrease in their energy as a function of the frequency value can be seen.

Against this background, the use of battery-powered motors in UAVs is attractive due to the low level of this type of interference. In this area of technology development, stepper, brushed and brushless motors (brushless direct current (BLDC)) can be distinguished, the latter of which, due to relatively high power, durability, and low EMI level, have found the greatest recognition in COTS UAVs [13–17].

When talking about electromagnetic interference of COTS UAVs, attention should also be paid to other sources of radio wave emission. These can be user-installed on-board devices, but above all, they are radio control signals. Due to commercial assumptions, these are frequencies from the ISM (industrial, scientific, and medical) bands. The characteristics of these frequencies in relation to commercial UAVs are presented in Table 1.

**Table 1**  
Frequency bands used to control commercial UAV

Frequency	Application	Distance	Data rate
433 MHz	radio control	medium	low
900 MHz	radio control	medium	low
2.4 GHz	video	short	medium
5.8 GHz	video	short	high

Before the measurements, we preliminarily confirmed that the electromagnetic waves generated by the propeller engines are negligible in our target frequency range (0.03 to 6 GHz). The motors are controlled by 12 kHz or 15 kHz pulse signals and the associated electromagnetic waves are limited to frequencies below 30 MHz. Also, the method of power supply, either with batteries or directly with alternating current (AC) sources, is almost irrelevant to the measurement results, so it was decided to power the UAV from batteries.

At frequencies below 200 MHz, disturbances related to the facility power supply are most common. They are related to the way the power lines are routed from the power source to the individual modules of the device and are related to the distribution of mass in printed circuit boards or are often the result of poor-quality power cables.

The frequencies of 2.4 GHz and 5.8 GHz (and sometimes 433 MHz and 900 MHz) are the frequencies that control the operation of the UAV. Due to the power value of the control signals, high levels of radiated disturbances may occur at frequencies that are harmonics for the control signals. This is the case for the 4.8 GHz frequency, where increased radiated emission values can be seen in some graphs (this harmonic should not exceed the permissible level – it is an undesirable emission).

At frequencies ranging from 200 MHz to 1000 MHz, disturbances may occur due to the presence of signals on the printed circuit board related to UAV control and on the printed circuit board related to transmitting the image from the camera. Unwanted emission is related to the operating frequencies of the clocks of microprocessor systems (microcontrollers) and the frequencies of control and control signals occurring in the UAV. Depending on the type of UAV, the frequencies of these signals may vary.

In turn, at frequencies above 1000 MHz, there may be disturbances related to the occurrence of signals originating from transmission standards with high transmission rates (high frequencies at which transmission takes place), e.g. USB 3.0 or wireless transmissions (as they occur in the device), e.g. LTE, Bluetooth Wi-Fi, etc.

## 2. THE LABORATORY TEST-BENCH

### 2.1. Subject of study

The following UAVs were tested:

1. Parrot AR Drone 2.0 (Sand Edition)
2. DJI Phantom 4 PRO V2
3. DJI Mavic 3 Fly More Combo
4. DJI FPV
5. DJI Ryze Tello
6. HGDRONEK66

The technical parameters of the tested UAVs are summarized in Table 2.

**Table 2**  
Technical parameters of the tested UAVs

Characteristic	Parrot AR Drone 2.0 [18]	DJI Phantom 4 PRO V2 [19]	DJI Mavic 3 Fly More Combo [20]	DJI FPV [21]	DJI Ryze Tello [22, 23]	HG-Dronek66 [24]
Frame and housing material	Nylon and carbon fiber	Magnesium alloy and reinforced plastic	Magnesium alloy and reinforced plastic	Plastic	Plastic	Carbon fiber
Motors	4 brushless motors, max speed 41 400 RPM (ab. 2700 kV <sup>1</sup> )	4 brushless motors, max speed ab. 10 000 RPM (ab. 700 kV)	4 brushless motors, max speed ab. 21 000 RPM (ab. 1400 kV)	4 brushless motors, max speed ab. 29 000 RPM (ab. 1400 kV)	4 brushed motors, max speed ab. 50 000 RPM (ab. 13.100 kV)	4 brushless motors, max speed ab. 8300 RPM (ab. 750 kV)

*Continued on the next page*

Table 2 [cont.]

Characteristic	Parrot AR Drone 2.0 [18]	DJI Phantom 4 PRO V2 [19]	DJI Mavic 3 Fly More Combo [20]	DJI FPV [21]	DJI Ryze Tello [22, 23]	HG-Dronek66 [24]
Functions and sensors	RTH, ultrasonic altimeter, pressure sensor, gyrometer, accelerometer	RTH, front, rear, bottom vision and ultrasonic, barometer, accelerometer	Smart RTH, forward range, top, bottom, and side sensors downward vision, downward ToF, barometer, accelerometer	RTH, forward range, downward vision, downward ToF, barometer, accelerometer	Optical flow, accelerometer, gyro, barometer, ToF	RTH, accelerometer, magnetometer, barometer, GPS
Communications and Control	2.4 GHz, GPS	2.400–2.483 GHz, 5.725–5.825 GHz, GPS, GLONASS.	2.400–2.4835 GHz, 5.725–5.850 GHz, GPS, Galileo, BeiDou	2.400–2.4835 GHz, 5.725–5.850 GHz GLONASS, GPS, Galileo	2.400–2.4835 GHz	2.4 GHz 433 MHz for telemetry
Flight battery	LiPo 1000 mAh, 11.1 V	LiPo4S 5870 mAh, 15.2 V	LiPo4S 5000 mAh, 15.4 V.	LiPo6S 2000 mAh, 22.2 V	LiPo 1100 mAh, 3.8 V	LiPo3S 5000 mAh, 11.1 V

RTH – return to home ToF – time of flight RPM – revolutions per minute

<sup>1</sup> 1 kV stands for “kilovolts per revolution” and it refers to the number of electrical revolutions per minute the motor will rotate, per volt of electrical power applied.

**2.2. Test conditions**

UAV tests were mostly conducted with the engines running in idle mode. In some cases, due to the specificity of launching the UAV, it was equivalent to raising the drone to a height of 1 m AGL (Table 3). In order to ensure communication on the control channels, the drone operator forced the flow of data using the available communication channels.

**Table 3**  
UAV launch conditions

Parrot AR Drone 2.0	DJI Phantom 4 PRO V2	DJI Mavic 3 Fly More Combo	DJI FPV	DJI Ryze Tello	HG-Dronek66
1 m AGL	idle	idle	idle	1 m AGL	idle

**2.3. Requirements and measurement procedure**

Depending on the intended use of unmanned aerial systems (UAV), the UAV manufacturer must meet the relevant requirements for products used in civil or military applications. Delegated Regulation 2019/945 defines the rules for placing on the internal market of the European Union and free movement in the EU of unmanned aerial systems intended for operation under the open category. These rules apply to, among others: the manufacturer’s obligation to assess a product conformity (i.e. UAV assessment) with the requirements set out in detail in the Annex to the Delegated Regulation and the relevant harmonized standards. Therefore, UAVs operated in the open category must meet the requirements of the Electromagnetic Compatibility Directive, according to which UAVs should emit as little electromagnetic interference as possible and be immune to such interference. UAVs operated in a military environment must meet the requirements of dedicated defense standards in force in a given country. For this reason, based on the defense standard for electromagnetic compatibility MIL-STD461G, a laboratory test-bench was compiled for testing the radiated emissions of unmanned aerial vehicles.

The block diagram of the laboratory test-bench for measuring radiated disturbances emitted by unmanned aerial vehicles is shown in Fig. 1. Figure 2 shows the arrangement of the tested UAV and the receiving antenna in the anechoic chamber. Measurements of radiated disturbances emitted by unmanned aerial vehicles consisted in measuring the electric field strength at a distance of 3 m from the UAV using measuring antennas and

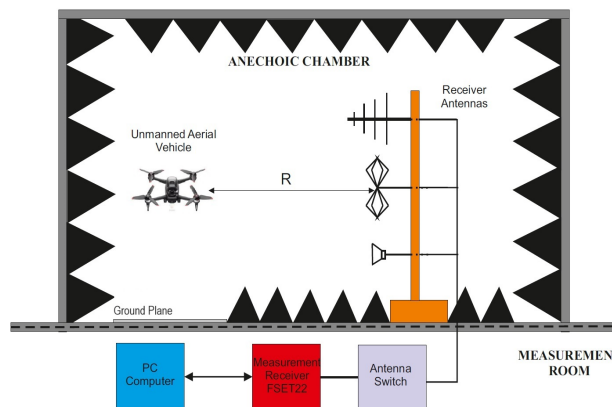


**Fig. 1.** Block diagram of the laboratory test bench for measuring radiated disturbances emitted by unmanned aerial vehicles

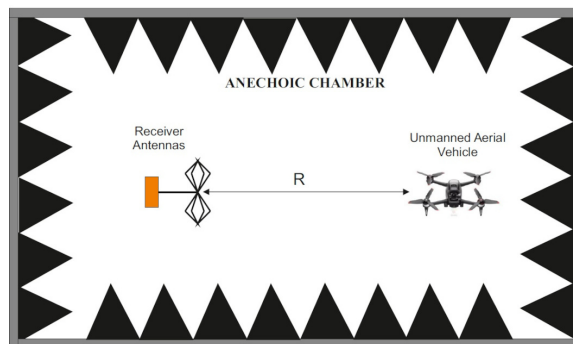


**Fig. 2.** Location of the tested unmanned aerial vehicle and receiving antennas in the anechoic chamber during the tests

a measuring receiver in the frequency range from 30 MHz to 6 GHz. Measurements were conducted for the vertical and horizontal polarization of the measuring antennas [25, 26].

The measurement site makes it possible to distinguish the electromagnetic disturbances caused by the UAV from the background of external electromagnetic disturbances. The usefulness of the measurement site in this respect was confirmed by measuring the background level of electromagnetic disturbances inside the anechoic chamber with the UAV turned off (the background level of electromagnetic disturbances should be at least 6 dB lower than the limit levels specified in the MIL-STD-461G standard). The view of the example configuration of the laboratory test bench during the tests is shown in Fig. 3.



**Fig. 3.** The view of an exemplary configuration of the laboratory test bench during the tests

In the discussed laboratory test bench, the tested object was installed on the reference ground plane imitating its real environment of use [25, 26].

In the discussed measurement procedure, the FSET22 measuring receiver manufactured by Rohde & Schwarz was used. This receiver, according to the manufacturer's declaration, meets all the requirements for measuring receivers used in these types of measurements. The defense standard MIL-STD-461G requires that the measuring receiver have a peak value detector and meet the requirements for the appropriate width of the RBW (resolution bandwidth) filter used, depending on the frequency range on which the measurement is conducted (10 kHz, 100 kHz, 1 MHz) and measurement time (20 ms).

During the measurements of the electromagnetic emission tests, the entire frequency range was scanned for each measurement. In the case of devices generating emissions at irregular intervals, the frequency scanning time should be increased to the value necessary to determine the presence of these emissions, which did not occur in the measurements conducted [25, 26]. The following set of measuring antennas was used to test electromagnetic emissions from unmanned aerial vehicles [25, 26]:

- In the frequency range from 30 MHz to 230 MHz, a double-cone antenna was used, in which the distance between the tops of the cones is 137 cm. The SAS 544 biconical antenna was used in the described laboratory test bench (Fig. 4a).
- In the frequency range from 230 MHz to 1000 MHz, a logo-periodic antenna was used. In the described laboratory test bench, the log-periodic antenna 3147(11966N) was used (Fig. 4b).

- In the frequency range from 1000 MHz to 6 GHz, the DRG 118/A horn antenna was used (Fig. 4c).

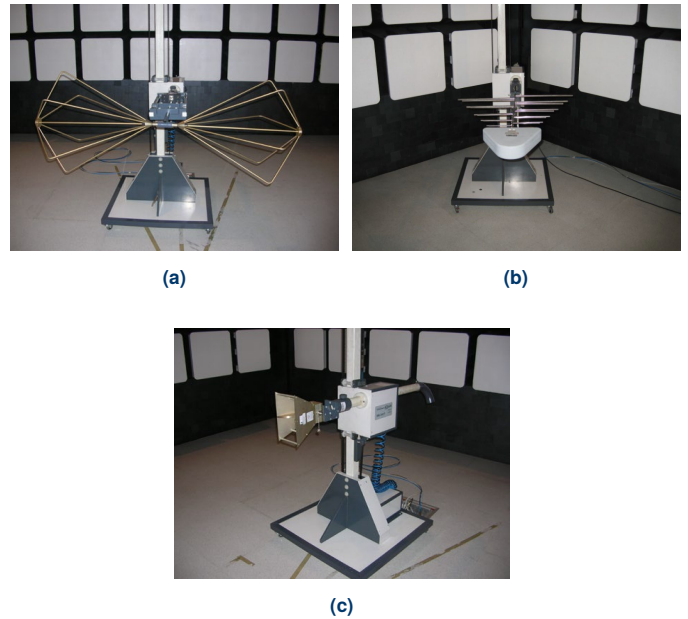


**Fig. 4.** The view of the measurement antennas: (a) SAS 544 biconical antenna; (b) 3147(11966N) log-periodic antenna; (c) DRG118/A horn antenna

The orientation of the test UAV relative to the reference ground corresponded to its orientation in practice. In the case of a research object in the form of an unmanned aerial vehicle, it is possible to place the UAV on the table, starting only the operation of the engines and systems on board, or to force it to hover over the surface of the reference ground plane. In the case of the conducted measurements, it was assumed that the conditions discussed in Section 2.2 are the normal mode of operation of the flying object. For this reason, in some cases, the test object was forced to hover over the surface of the reference ground plane after its start. The location of the tested UAV above the reference ground plane is shown in Fig. 5.

In order to improve the measurements, the EMC 32 application produced by Rohde & Schwarz was used to control the

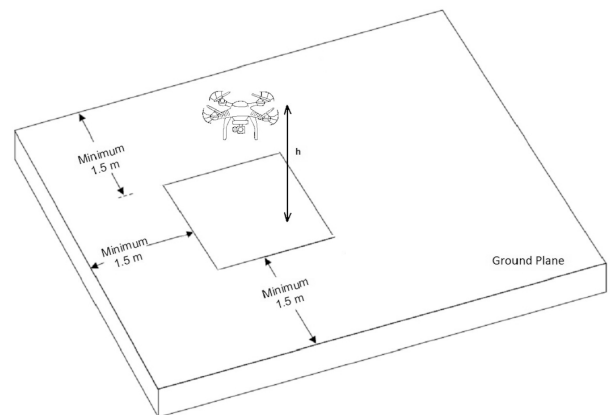


**Fig. 5.** Measuring system for testing unmanned aerial vehicles

measurement process. This program enables the automatic execution of basic preparatory activities, the implementation of the measurements themselves, and the preparation of appropriate charts presenting the obtained results. In addition, the application allows you to perform a preliminary analysis of the obtained results.

In order to measure the radiated emission generated by the UAV, the following steps were performed:

- switching on the power supply of the measuring instruments and leaving them in this state for the time necessary to obtain proper stability,
- arrangement of the set of measuring antennas used during the test,
- checking whether the requirements regarding the background of environmental disturbances are met and preparing a spectrogram of the background disturbances,
- starting the retuning of the measuring receiver, with properly set tuning parameters in accordance with the requirements specified in the standard,
- authentication of the measurement track and checking the electrical continuity of the measurement antennas,
- launching the test object and setting it in the appropriate operating mode,
- taking measurements for each of the previously determined antenna positions for horizontal and vertical polarization,
- rotate the object 90 degrees clockwise and perform item g) again. End the measurements after performing a series of measurements for all 4 sides of the UAV (front, back, left side, right side).

#### 2.4. Measurement uncertainty budget

The uncertainty budget is a statement of measurement uncertainty, the components of that measurement uncertainty, and how they are calculated and combined. It contains data on the probability distribution of individual components, as well as the method of calculating the combined uncertainty and the calibration result. An uncertainty budget facilitates taking into account all components of measurement uncertainty and sensitivity coefficients that were adopted for calculations. The uncertainty components can be divided into two types depending on the method of their determination: “type A” and “type B”. The type A method of calculating standard uncertainty consists of the statistical analysis of a series of observations. The standard uncertainty in this case is the standard deviation. This method requires a large number of measurement repetitions and applies to random errors. It is used when it is possible to perform many repetitions of the measurement of the same quantity under identical measurement conditions. The type B method of calculating the standard uncertainty involves determination using scientific analysis based on all available information on the variability of the input quantity, e.g. based on calibration certificates of measuring equipment.

When determining the measurement uncertainty budget for measurements of radiated disturbances (E) emitted by unmanned aerial vehicles, the following input quantities should be taken into account [27, 28]:

- receiver indications ( $V_r$ , determined by B method),

- attenuation of the connection between the antenna and the receiver ( $a_c$ , determined by A method),
- antenna coefficient ( $F_{AMN}$ , determined by B method),
- input quantities associated with the receiver:
  - accuracy of receiver sinusoidal voltage measurements ( $\delta V_{sw}$ , determined by B method),
  - the amplitude response of the receiver to the pulses ( $\delta V_{pa}$ , determined by B method),
  - the response of the receiver to pulses with a variable repetition rate ( $\delta V_{pr}$ , determined by B method),
  - the receiver noise ( $\delta V_{nf}$ , determined by B method),
- patch mismatch: antenna-receiver ( $\delta M$ , determined by B method),
- input quantities related to the antenna:
  - AF (antenna factor) frequency interpolation ( $\delta F_{af}$ , determined B method),
  - change of AF as a function of frequency ( $\delta F_{ah}$ , determined by B method),
  - directionality difference ( $\delta F_{adir}$ , determined by B method),
  - the location of the phase center ( $\delta F_{aph}$ , determined by B method),
  - orthogonal component ( $\delta F_{acp}$ , determined by B method),
  - symmetry ( $\delta F_{abal}$ , determined by B method),
- the imperfection of the laboratory test bench ( $\delta A_N$ , determined by A method),
- measuring distance ( $\delta d$ , determined by A method),
- UAV suspension height ( $\delta h$ , determined by A method),
- influence of ambient noise ( $\delta E_{amb}$ , determined by A method) [27, 28].

The model equation for the measured quantity E, taking into account the main sources of uncertainty in the measuring equipment, gives a mathematical definition of the measured quantity and is calculated from the relationship:

$$\begin{aligned}
 E = & V_r + a_c + F_{AMN} + \delta V_{SW} + \delta V_{pa} + \delta V_{pr} + \delta V_{nf} \\
 & + \delta M + \delta F_{af} + \delta F_{ah} + \delta F_{adir} + \delta F_{aph} + \delta F_{acp} \\
 & + \delta F_{abl} + \delta A_N + \delta d + \delta h + \delta E_{amb}.
 \end{aligned} \quad (1)$$

In order to determine the expanded uncertainty, several steps must be performed. For the identified sources of uncertainty, input quantities ( $x_i$ ) were determined for which the standard uncertainty ( $U(x_i)$ ) was determined based on the methods of its determination (type A or type B) and standardized in [dB]. When determining the standard uncertainty for input quantities ( $x_i$ ) using the type B method, mainly calibration certificates for measuring equipment were used, where these values were read directly in [dB]. When determining the standard uncertainty for input quantities ( $x_i$ ) using the type A method, standard deviations for the measured quantities were determined using repeated measurements and then transformed into [dB]. Then, probability density distributions were adopted for all input quantities, which depend on their source. Each probability distribution is assigned a divisor ( $d$ ) needed to determine the standard deviation. After determining the probability distributions and their assigned divisors, standard deviations were estimated for all

input quantities based on the formula:

$$u(x_i) = \frac{U(x_i)}{d}. \quad (2)$$

In the next step, when determining the expanded measurement uncertainty, the sensitivity coefficient related to the input quantity was determined. It is a partial derivative that describes how the estimate of the output varies with changes in the values of the input estimates. This parameter describes the relationship:

$$c_i = \frac{\partial f}{\partial x_i} = \frac{\partial f}{\partial X_i} \Big|_{X_1 = x_1 \dots X_N = x_N}, \quad (3)$$

where:  $c_i$  – sensitivity coefficient,  $x_i$  – an estimate of the input quantity,  $X_i$  – the value of the input quantity.

Its contribution to the expanded standard uncertainty is determined by the relationship:

$$u_i(y) = c_i \cdot u(x_i), \quad (4)$$

where:  $u_i(y)$  – contribution to the composite standard uncertainty,  $c_i$  – sensitivity coefficient,  $u(x_i)$  – standard uncertainty,

After determining the value of  $u_i(y)$  for all input values of the uncertainty budget, the value of the combined standard uncertainty  $u_s(y)$  was calculated from the formula:

$$u_s(y) = \sqrt{\sum (c_i \cdot u(x_i))^2}, \quad (5)$$

and then, for a specific expansion factor that reflects a certain level of confidence ( $k = 2$ ), the value of the expanded measurement uncertainty for the laboratory test bench was determined using the formula:

$$U(y) = k \cdot u_s(y). \quad (6)$$

Table 4 presents the value of the determined measurement uncertainty budget for the developed laboratory test bench for the measurement of radiated emissions generated by unmanned

**Table 4**

Uncertainty budget for the measurement of the radiated emission in the frequency range from 30 MHz to 6 GHz

Input values	$X_i$	Uncertainty $x_i$ $U(x_i)$		Divisor by a probability distribution $d$	Sensitivity factor	$c_i \cdot u(x_i)$
		$x_i$ [dB]	Probability distribution		$c_i$	
		±				$u_i(y)$ [dB]
Receiver indications	$V_r$	0.600	Normal $k = 1$	1.000	1	0.600
Attenuation path: antenna receiver	$a_c$	0.100	Normal $k = 2$	2.000	1	0.050
Antenna coefficient	$F_{AMN}$	2.000	Normal $k = 2$	2.000	1	1.000
Receiver correction factors:						
Sine voltage	$\delta V_{sw}$	0.400	Normal $k = 2$	2.000	1	0.200
Amplitude response to impulses	$\delta V_{pa}$	1.000	Rectangular	1.732	1	0.577
Response to pulses with a variable repetition rate	$\delta V_{pr}$	1.000	Rectangular	1.732	1	0.577
Proximity to self-noise	$\delta V_{nf}$	0.700	Normal $k = 1$	1.000	1	0.700
Path mismatch: antenna receiver	$\delta M$	0.023	U type	1.414	1	0.016
Antenna correction factors:						
AF frequency interpolation	$\delta F_{af}$	0.300	Triangular	2.449	1	0.122
AF change as a function of height	$\delta F_{ah}$	1.000	Normal $k = 1$	1.000	1	1.000
Difference in directivity	$\delta F_{adir}$	0.000	Normal $k = 1$	1.000	1	0.000
Location of the phase center	$\delta F_{aph}$	0.100	Normal $k = 1$	1.000	1	0.100
Orthogonal component	$\delta F_{acp}$	0.000	Normal $k = 1$	1.000	1	0.000
Symmetry	$\delta F_{abal}$	0.300	Normal $k = 1$	1.000	1	0.300
Measuring stand imperfection	$\delta A_N$	1.000	Triangular	2.449	1	0.408
Measuring distance	$\delta d$	0.100	Rectangular	1.732	1	0.058
UAV suspension height	$\delta h$	0.010	Normal $k = 2$	2.000	1	0.005
The influence of ambient noise	$\delta E_{amb}$	0.010	Normal $k = 1$	1.000	1	0.010
$\sqrt{\sum (c_i \cdot u(x_i))^2}$						3.845
$u_s(y) = \sqrt{\sum (c_i \cdot u(x_i))^2}$						1.961
$k =$						2.000
Extended uncertainty $U(y)$						3.922
Expanded uncertainty for the measurement stand $U(y)$						3.9

aerial vehicles in the frequency range from 30 MHz to 6 GHz. The expanded uncertainty for a laboratory test bench for measuring radiated emissions from UAVs is 3.9 dB.

### 3. MEASUREMENT RESULTS AND DISCUSSION

Figures 6 to 11 show the measurement results for each of the six tested UAVs in the frequency band from 30 MHz to 6 GHz. The presented values of radiated emission of all UAVs are the maximum values obtained during the implementation of eight measurement series consisting of measurements from four sides of the object (front, back, left side, right side) and with two polarizations of the receiving antenna (vertical and horizontal) for all frequencies. The level of radiated interference was compared to the limit values introduced by the civil standard EN-55011 and the military standard MIL-STD-461G. In addition, the ambient electromagnetic level was applied in red. In the ambient electromagnetic level graph, we can see two clear changes in levels at the frequencies at which the measurement antennas were changed. The measurements were made using three measurement antennas in three different frequency bands (30 MHz–230 MHz, 230 MHz–1000 MHz, 1 GHz–6 GHz). Each antenna is characterized by different values of antenna factor (AF), which affect the ambient electromagnetic level. The lower the antenna coefficient, the lower the ambient electromagnetic level. The antenna in the 230-1000 MHz band is characterized by low antenna factor values compared to other antennas used, which reduces the ambient electromagnetic level. In this frequency band, it was also possible to switch on an additional preamplifier in the measurement receiver, thanks to which a significant reduction in the ambient electromagnetic level was observed. Before a detailed analysis of the measurement results, it is worth paying attention to the obvious exceeding of the limits at the starting frequencies, i.e. 2.4 GHz, and 5.8 GHz. Figures 6 to 11 show the values of radiated emission from the UAV measured at a distance of 3 m from the UAV, which were determined with a measurement uncertainty of  $\pm 3.9$  dB. It should be understood that for each frequency the radiated emission value is  $E = e \pm 3.9$  dB.

Apart from the control frequencies, the levels of radiated disturbances do not exceed the admissible levels recommended by the civil standard in any frequency range. However, when it comes to military recommendations (more demanding), the values of undesirable emissions exceed the permissible levels in the range of about 40 MHz and about 200 and 400 MHz (Fig. 6).

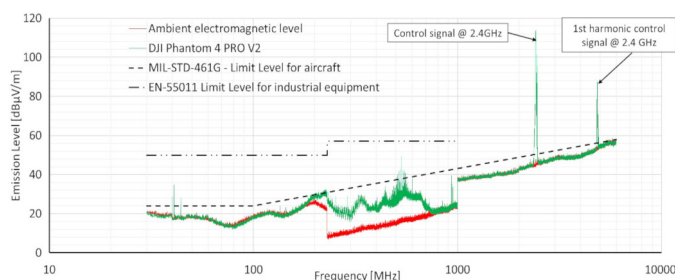


**Fig. 6.** Radiated emission disturbance values produced by the DJI Phantom 4 PRO V2 drone in the frequency range from 30 MHz to 6000 MHz

The values of radiated emission disturbances for DJI FPV (Fig. 7) do not exceed the levels recommended by civil and military standards in any frequency range. The exceedances of the permissible levels visible in the figure are the desired emissions related to the exchange of control information.

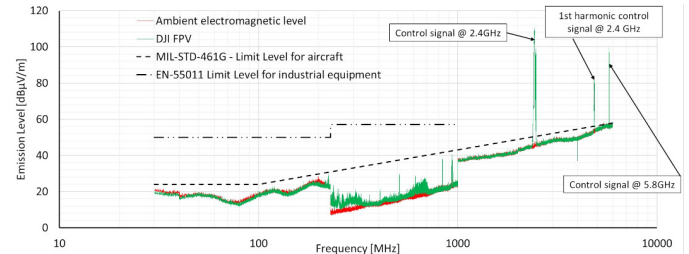


**Fig. 7.** Radiated emission disturbance values produced by the DJI FPV drone in the frequency range from 30 MHz to 6000 MHz

Observing the measurement results presented in Fig. 8 for the HGDRONEK66 unmanned aerial vehicle, it can be concluded that the permissible levels specified in both military and civil standards have been exceeded. The highest exceedances occur in the range from 100 MHz to 900 MHz. This situation may result from the fact that the tested type of UAV is a development kit intended for testing new functionalities.

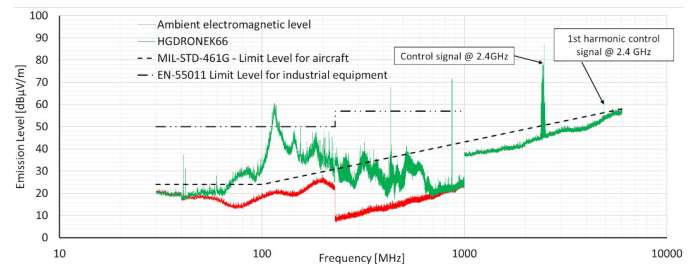


**Fig. 8.** Radiated emission disturbance values produced by the HGDRONEK66 drone in the frequency range from 30 MHz to 6000 MHz

As can be seen in Fig. 9, exceeding the levels of permissible radiated emissions for the Mavic 3 Fly More Combo UAV occurs in similar ranges as for the DJI Phantom 4 PRO V2 (Fig. 6).

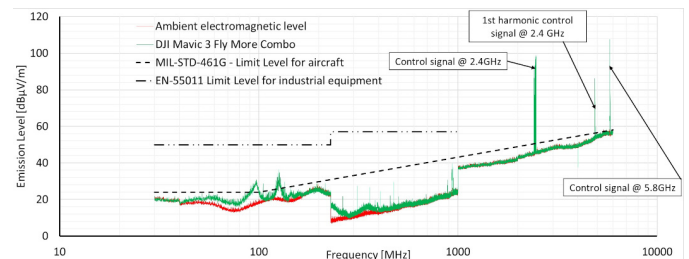


**Fig. 9.** Radiated emission disturbance values produced by the DJI Mavic 3 Fly More Combo drone in the frequency range from 30 MHz to 6000 MHz

The results for a simple AR Drone 2.0 UAV shown in Fig. 10 show relatively small exceedances of the military emission limits in the range of about 800 MHz.

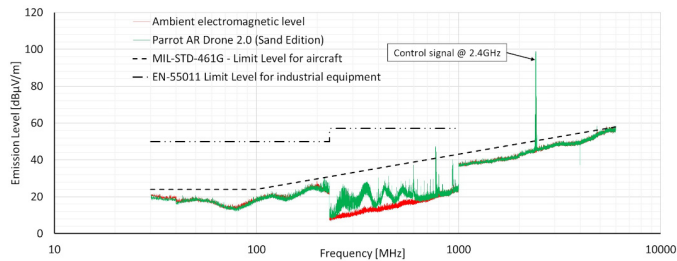


**Fig. 10.** Radiated emission disturbance values produced by the Parrot AR Drone 2.0 (Sand Edition) drone in the frequency range from 30 MHz to 6000 MHz

A simple UAV of the DJI Ryze Tello type (Fig. 11) is characterized by a slight exceedance of the military emission limits in the frequency range of about 1.8 GHz and 5 GHz.

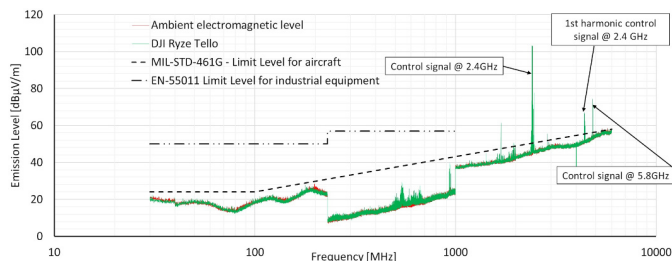


**Fig. 11.** Radiated emission disturbance values produced by the DJI Ryze Tello drone in the frequency range from 30 MHz to 6000 MHz

#### 4. UAV ELECTROMAGNETIC DISTURBANCES ATTENUATING METHODS

Electromagnetic interference is mainly caused by the way of interference and the device being interfered with. Electronic devices that generate interference in UAV systems include flight control systems, various types of measurement modules (inertial measurement unit (IMU), GPS locator, barometer, magnetic compass, etc.), and signal receivers. Therefore, the essence of designing anti-electromagnetic interference systems for UAVs mainly lies in how to protect these devices [29].

There are two ways in which interference can occur in UAVs: via radio coupling and conductive coupling. RF coupling means that electromagnetic waves escape from the cabin through ventilation windows and other gaps in the UAV body and equipment casing, transmission line interfaces and connection gaps, or electromagnetic coupling between onboard electronic equipment, due to interference in the equipment and electronic circuits. Forward coupling means that electromagnetic waves induce a current in other equipment, such as antennas or external circuits, and conduct it along the power and signal circuits. According to the above interference methods, shielding and filtering methods are mainly used to protect electricity-powered drones, which are sources of interference [30].

##### 4.1. Shield

Electromagnetic wave shielding technology mainly uses absorbent (absorbing) materials to block electromagnetic wave in-

terference. In actual use, shielding technology can only slightly reduce electromagnetic waves through absorption and reflection, but cannot effectively block them. In traditional electromagnetic shielding, components made of conductive materials or ferromagnetic materials are commonly used to shield and isolate protected objects in order to control the induction and radiation of electric fields, magnetic fields, and electromagnetic waves from one area to another. However, due to the lightweight requirements of drones, conventional shielding materials (copper, iron, aluminum, and other metals) are generally not used to produce drone shells.

Currently, UAV shell parts typically use structural plastics or carbon fiber composite materials. Engineering plastics do not have much protection against electromagnetic interference. However, some researchers have applied a layer of metal [31] or other electromagnetic wave shielding coatings [32] to the plastic structural shell to turn the processed plastic shell into a Faraday shield to achieve a certain anti-electromagnetic interference effect. This approach is simple in operation and design, and the production cost is generally low, but there are corresponding shortcomings. For example, coating scratches may damage the shielding. During thermal cycling, the coating may degrade due to heat and cause other coating adhesion problems. It may be necessary to add additional protective surfaces to avoid oxidation of the coating. Therefore, some researchers have changed their attention to the development of carbon fiber composite materials with electromagnetic shielding properties [33–36].

Without adding special parts inside the drone, use appropriate insulating materials to fill all the gaps in the drone to prevent electromagnetic waves from entering. These filler materials include wire mesh pads, conductive fabric pads, soft metals, etc. Adding a shielding layer near electronic components can also reduce electromagnetic interference. For example, use aluminum foil for the entire package and use a shielded twisted pair in the signal circuit.

You can also reduce the impact of electromagnetic interference by optimizing the design of your drone. For example, keep the drone key components, flight control system, and measurement system away from the interface and gap to weaken electromagnetic waves in these parts. Separate the instrument cord from the power cord as much as possible.

##### 4.2. Filter

Filtering is a method of removing interfering signals. Filtering refers to the technology of filtering electromagnetic interference energy in the conductive coupling and maintaining the operating level in the line. For the energy coupled in from the antenna part, a band-pass filter can be used on an external interface such as an antenna to filter and adjust the received signal. In the case of energy drawn from external lines, power filters can be used. To improve the high-frequency interference signal, a commonly used electromagnetic interference filter is the ferrite ring magnetic filter [37]. Depending on the interference suppression frequency, select ferrite materials with different permeability. The higher the permeability of the ring magnet, the greater the impedance at low frequencies and the smaller the impedance at high frequencies. A ferrite bead can be considered a resistor



whose resistance changes with frequency. According to the frequency characteristics of the electromagnetic wave, nickel-zinc ferrite or manganese-zinc ferrite can be selected.

The high-frequency characteristics of the former are better than the latter. The higher the magnetic permeability of ferrite, the greater the impedance at low frequencies and the lower the impedance at high frequencies. Therefore, nickel-zinc ferrite should be used to suppress high-frequency interference. Otherwise, use manganese-zinc ferrite. It is also possible to place manganese-zinc and nickel-zinc ferrite on the same wire harness at the same time, making the frequency band of interference that can be suppressed wider. The greater the difference between the inner and outer diameters of the magnetic ring and the greater the longitudinal height, the greater the impedance, but the inner diameter of the magnetic ring must be tightly packed to avoid magnetic leakage. The mounting location of the magnetic ring should be as close to the source of interference or interface as possible.

## 5. CONCLUSIONS

Summarizing the results of tests and sample analyses of the COTS UAV, and in particular, assessing their usefulness in civil and military reconnaissance activities related to the study of the activity of radio emission sources in the 30 MHz to 6 GHz band, it can be confirmed that devices whose engine system is based on brushless technology emits relatively low levels of radiated interference. These disturbances are greater for amazingly simple structures and small for most popular DJI UAVs. Importantly, the interference emitted in the discussed range is not only exceeded for the civil standard but also meets the requirements recommended by the MIL-STD-461G military standard, which allows the COTS UAV to be used as a carrier for specialized military electronic systems (not forgetting interference from control channels). It is important to eliminate undesirable emissions with too high levels by using various types of electromagnetic protection in the form of filters and electromagnetic screens, using appropriate connections on printed circuit boards, and proper grounding.

## ACKNOWLEDGEMENTS

This work was financed by the Military University of Technology under the UGB/22-860/2023 and UGB/22-859/2023 research projects.

## REFERENCES

- [1] D. Srivastava, R. Pakkar, A. Langrehr, and C. Yamane, "Adaptable UAV Swarm Autonomy and Formation Platform," in *2019 IEEE Aerospace Conference*, USA, Mar. 2019, pp. 1-6, doi: [10.1109/AERO.2019.8741683](https://doi.org/10.1109/AERO.2019.8741683).
- [2] M.A. Ma'sum, M.K. Arrofi, G. Jati, F. Arifin, M.N. Kurniawan, pp. Mursanto, and W. Jatmiko, "Simulation of intelligent Unmanned Aerial Vehicle (UAV) For military surveillance," in *2013 International Conference on Advanced Computer Science and Information Systems (ICACSIS)*, Indonesia, Sept. 2013, pp. 161-166, doi: [10.1109/ICACSIS.2013.6761569](https://doi.org/10.1109/ICACSIS.2013.6761569).
- [3] E. Skjervold and O. T. Hoelsreter, "Autonomous, Cooperative UAV Operations Using COTS Consumer Drones and Custom Ground Control Station," in *2018 IEEE Military Communications Conference (MILCOM)*, USA, Oct. 2018, pp. 1-6, doi: [10.1109/MILCOM.2018.8599684](https://doi.org/10.1109/MILCOM.2018.8599684).
- [4] T. Coffey and J.A. Montgomery, "The Emergence of Mini UAVs for Military Applications," *Def. Horiz.*, no. 22, pp. 1-8, Dec. 2002.
- [5] S.J. Kim and N.J. Sheikh, "Acquisition of Commercial-Off-The-Shelf (COTS) Unmanned Aerial Systems: Lessons Learned from the South Korean Military," in *2022 Portland International Conference on Management of Engineering and Technology (PICMET)*, USA, pp. 1-7, Aug. 2022, doi: [10.23919/PICMET53225.2022.9882659](https://doi.org/10.23919/PICMET53225.2022.9882659).
- [6] M. Gargalakos, "The role of unmanned aerial vehicles in military communications: application scenarios, current trends, and beyond," *J. Def. Model. Simul.-Appl. Methodol. Technol.*, July 2021, doi: [10.1177/15485129211031668](https://doi.org/10.1177/15485129211031668).
- [7] P. Stodola, J. Kozubek and J. Drozd, "Using Unmanned Aerial Systems in Military Operations for Autonomous Reconnaissance," in *Modelling and Simulation for Autonomous Systems. MESAS 2018. Lecture Notes in Computer Science*, vol. 11472, pp. 514-529, Oct. 2018, doi: [10.1007/978-3-030-14984-0\\_38](https://doi.org/10.1007/978-3-030-14984-0_38).
- [8] A. Gupta, T. Afrin, E. Scully and N. Yodo, "Advances of UAVs toward Future Transportation: The State-of-the-Art, Challenges, and Opportunities," *Future Transp.*, vol. 1, no. 2, pp. 326-350, 2021. doi: [10.3390/futuretransp1020019](https://doi.org/10.3390/futuretransp1020019).
- [9] C. Marczok, U. Maaß, E. Hoene, I. Ndiip, K.D. Lang, and D. Haselberg, "Analysis and improvement of a spark plug for less radiated electromagnetic emissions," in *2014 International Symposium on Electromagnetic Compatibility*, Sweden, Sept. 2014, pp. 385-390, doi: [10.1109/EMCEurope.2014.6930937](https://doi.org/10.1109/EMCEurope.2014.6930937).
- [10] F. Pavlovič, "Commutator motors as EMI sources," in *SPEEDAM 2010*, Italy, 2010, pp. 1789-1793, doi: [10.1109/SPEEDAM.2010.5545039](https://doi.org/10.1109/SPEEDAM.2010.5545039).
- [11] H. Diamond and F.G. Gardner, "Engine-Ignition Shielding for Radio Reception in Aircraft," *Proc. Inst. Radio Eng.*, vol. 18, no. 5, pp. 840-861, May 1930, doi: [10.1109/JRPROC.1930.222075](https://doi.org/10.1109/JRPROC.1930.222075).
- [12] M.A. Jabbar and M.A. Rahman, "Radio frequency interference of electric motors and associated controls," *IEEE Trans. Ind. Appl.*, vol. 27, no. 1, pp. 27-31, Jan.-Feb. 1991, doi: [10.1109/28.67528](https://doi.org/10.1109/28.67528).
- [13] D.L. Gabriel, J. Meyer, and F. Du Plessis, "Brushless DC motor characterisation and selection for a fixed wing UAV," in *IEEE Africon'11*, Sept. 2011, pp. 1-6, doi: [10.1109/AFRCON.2011.6072087](https://doi.org/10.1109/AFRCON.2011.6072087).
- [14] M.K. Pandey, A. Tripathi, and B. Dwivedi, "A technique to minimize the effect of current harmonics in a brushless DC motor drive," in *2015 IEEE 10th Conference on Industrial Electronics and Applications (ICIEA)*, New Zealand, June 2015, pp. 702-706, doi: [10.1109/ICIEA.2015.7334199](https://doi.org/10.1109/ICIEA.2015.7334199).
- [15] Z. Sun, L. Zhong, X. Cheng, and J. Guo, "Analysis of Electromagnetic Interference and Restraining Measures of Brushless DC Motor Drive System," in *2023 IEEE 3rd International Conference on Power, Electronics and Computer Applications (ICPECA)*, China, Jan. 2023, pp. 382-385, doi: [10.1109/ICPECA56706.2023.10076028](https://doi.org/10.1109/ICPECA56706.2023.10076028).

- [16] O. Araar, M.Z. Mimouni, K. Fellah, and H. Osmani, "Identification & control of a multicopter UAV in the presence of actuator asymmetry," in *2017 25th Mediterranean Conference on Control and Automation (MED)*, Malta, July 2017, pp. 1035–1040, doi: [10.1109/MED.2017.7984254](https://doi.org/10.1109/MED.2017.7984254).
- [17] A.H. Zulkipli, T. Raj, F.H. Hashim, and A.B. Huddin, "Characterization of DC brushless motor for an efficient multicopter design," in *2016 International Conference on Advances in Electrical, Electronic and Systems Engineering (ICAEES)*, Malaysia, 2016, pp. 586–591, doi: [10.1109/ICAEES.2016.7888114](https://doi.org/10.1109/ICAEES.2016.7888114).
- [18] "Parrot AR Drone 2.0." Productz. [Online]. Available: <https://productz.com/en/parrot-ar-drone-2-0/p/bVaW> (accessed: 22-05-2023).
- [19] Phantom 4 Pro User Manual v.2.0, 2021.11.
- [20] DJI Mavic 3 User Manual v1.0, 2021.11.
- [21] DJI FPV User Manual v1.2, 2021.06.
- [22] Tello User Manual v1.4, 2018.09.
- [23] S. Pikalov, E. Azaria, S. Sonnenberg, B. Ben-Moshe, and A. Azaria, "Vision-Less Sensing for Autonomous Micro-Drones," *Sensors*, vol. 21, no. 16, p. 5293, Aug. 2021, doi: [10.3390/s21165293](https://doi.org/10.3390/s21165293).
- [24] "NXP HoverGames drone kit including RDDRONE-FMUK66 and peripherals," NPX. [Online]. Available: <https://www.nxp.com/design/designs/nxp-hovergames-drone-kit-including-rd-drone-fmuk66-and-peripherals:KIT-HGDRONEK66> (accessed: 22-05-2023).
- [25] *Requirements for the control of electromagnetic interference characteristics of subsystems and equipment*, MIL-STD-461G, Department of Defense Interface Standard, Dec. 2015.
- [26] R. Przesmycki and R. Kubacki, "EMC requirements for equipment used in the Polish army – Impact of changes the NO-06-A500:2012 standard on the measuring results," in *2014 20th International Conference on Microwaves, Radar and Wireless Communications (MIKON)*, Poland, 2014, pp. 1–4. doi: [10.1109/MIKON.2014.6899936](https://doi.org/10.1109/MIKON.2014.6899936).
- [27] *Wymagania dotyczące aparatury pomiarowej i metod pomiaru zaburzeń radioelektrycznych oraz odporności na zaburzenia – Część 4-2: Niepewności, statystyka i modelowanie poziomu dopuszczalnego – Niepewność aparatury pomiarowej*, PN-EN 55016-4-2:2011/A1, Polski Komitet Normalizacyjny, 2014.
- [28] B.N. Taylor and C.E. Kuyatt, "NIST Technical Note 1297, Guidelines for Evaluating and Expressing the Uncertainty of NIST Measurement Results," U.S. Department of Commerce Technol. Administration, National Institute of Standards and Technology, Sep. 1994.
- [29] X. Zhang, X. Wang, and Y. Wei, "Research of Security Strategy of UAV Board Data link," *Comput. Secur.*, vol. 3, pp. 62–64, 2008.
- [30] D. Zhang, Y. Chen, and E. Cheng, "Effects of Electromagnetic Interference (EMI) on Information Link of UAV," *Trans. Beijing Inst. Technol.*, vol. 39, pp. 756–762, 2019.
- [31] H. Weilin, "Alcohol-Soluble Electromagnetic Wave Shielding Coating," Guangdong Dewey Technology Co Ltd, Chinese Patent CN101880499.
- [32] D.D.L. Chung, "Carbon materials for structural self-sensing, electromagnetic shielding and thermal interfacing," *Carbon*, vol. 50, pp. 3342–3353, 2012, doi: [10.1016/j.carbon.2012.01.031](https://doi.org/10.1016/j.carbon.2012.01.031).
- [33] L. Chen *et al.*, "Mechanical and electromagnetic shielding properties of carbon fiber reinforced silicon carbide matrix composites," *Carbon*, vol. 95, pp. 10–19, Dec. 2015, doi: [10.1016/j.carbon.2015.08.011](https://doi.org/10.1016/j.carbon.2015.08.011).
- [34] Y. Zhan, Z. Long, X. Wan, J. Zhang, S. He, and Y. He, "3D carbon fiber mats/nano-Fe<sub>3</sub>O<sub>4</sub> hybrid material with high electromagnetic shielding performance," *Appl. Surf. Sci.*, vol. 444, pp. 710–720, Jun. 2018, doi: [10.1016/j.apsusc.2018.03.006](https://doi.org/10.1016/j.apsusc.2018.03.006).
- [35] Y. Jia, K. Li, L. Xue, J. Ren, S. Zhang, and H. Li, "Mechanical and electromagnetic shielding performance of carbon fiber reinforced multilayered (PyC-SiC) n matrix composites," *Carbon*, vol. 111, pp. 299–308, Jan. 2017, doi: [10.1016/j.carbon.2016.10.004](https://doi.org/10.1016/j.carbon.2016.10.004).
- [36] S. Tanabe, Y. Murata, H. Chishaki, and T. Shimato, "3D-MoM analysis of radio frequency noise radiation from HVDC converter station," in *1999 IEEE International Symposium on Electromagnetic Compatibility. Symposium Record, USA, 1999*, pp. 980–985 vol. 2, doi: [10.1109/ISEMC.1999.810199](https://doi.org/10.1109/ISEMC.1999.810199).
- [37] Y. Chen, D. Zhang, E. Cheng, and X. Wang, "Investigation on susceptibility of UAV to radiated IEMI," in *2018 IEEE International Symposium on Electromagnetic Compatibility and 2018 IEEE Asia-Pacific Symposium on Electromagnetic Compatibility (EMC/APEMC)*, Singapore, 2018, pp. 718–722, doi: [10.1109/ISEMC.2018.8393875](https://doi.org/10.1109/ISEMC.2018.8393875).